CHEMMEDCHEM

CHEMISTRY ENABLING DRUG DISCOVERY

Accepted Article

Title: Assembly of fully substituted 2H-indazoles catalyzed by Cu2O rhombic dodecahedra and evaluation of anti-cancer activity

Authors: Kaushik Chanda, Venkatraman Manickam, and Rajeeva Lochana P

To be cited as: *ChemMedChem* 10.1002/cmdc.201800707

Link to VoR: http://dx.doi.org/10.1002/cmdc.201800707

A Journal of

ChemPubSoc Europe

WILEY-VCH

www.chemmedchem.org

FULL PAPER WILEY-VCH

Assembly of fully substituted 2*H*-indazoles catalyzed by Cu_2O rhombic dodecahedra and evaluation of anti-cancer activity

Rajeeva Lochana Panchangam,[a] Venkatraman Manickam,*[a] and Kaushik Chanda*[b]

[a] Rajeeva Lochana Panchangam, Prof. Venkatraman Manickam
Department of Biosciences
School of Bioscience and Technology
Vellore Institute of Technology
Vellore-632014, India
E-mail: venkatraman.m@vit.ac.in

[b] Prof. Kaushik Chanda
Department of Chemistry
School of Advanced Sciences
Vellore Institute of Technology
Vellore-632014, India
E-mail: chandakaushik1@gmail.com

Supporting information for this article is given via a link at the end of the document.

Abstract: Simultaneous C-N, and N-N bond forming methods for the one-pot transformation are highly demanding in synthetic organic chemistry. In this report, we demonstrated the Cu_2O rhombic dodecahedra catalyzed synthesis of 2*H*-indazoles with very good to excellent yields from readily available chemicals. This one-pot procedure involves the Cu_2O nanoparticle catalyzed consecutive C-N, and N-N bond formation followed by the cyclization to obtain *2H*-indazoles with broad substrate scope and high functional group tolerance. Various cell based bio-assay studies demonstrated that 2*H*-indazoles inhibits the growth of cancer cells typically through induction of apoptosis in a dose dependent manner. Moreover 2*H*-indazoles are capable of inhibiting cancer cell migration and invasion when tested in MDA-MB-468 cell line. Thus we show here that 2*H*-indazoles have potent *in-vitro* anticancer activity which can be explored further.

Introduction

Heterocyclic compounds obtained by diversity-oriented synthesis are widely found among natural products and bioactive molecules and have vast array of application in numerous fields.[1] Over the last decade researchers are paying more attention for indazole derivatives in drug discovery research as it is acts as bioisosteres of indoles and benzimidazoles.[2] Molecules with 2*H*-indazole moieties have a wide range of biological properties such as antitumor,[3] HIV-protease inhibition,[4] anti-inflammatory,[5] and modulatory role on estrogen receptors.[6] Moreover, in addition to these biological activities, indazole scaffolds also exhibit photophysical properties for tentative theranostic applications.[7] Evidently the core structure of 2*H*-indazole has been found in many drugs such as pazopanib (A), and niraparib (B) and other covalent inhibitor (C) while targeting the drug resistant, epidermal growth factor receptor (EGFR) over expressing tumors as shown in Figure 1.[8] Moreover the related heterocycles have also been used in Ru catalyzed C-H activation.[9]

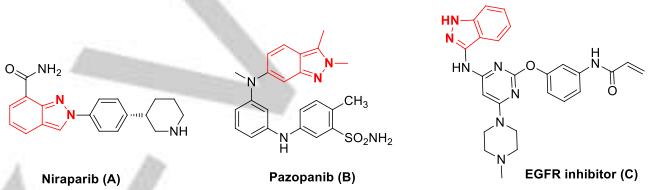

Figure 1. Biologically active 2*H*-indazole moieties.

In view of their wide ranging bioactivities, several synthetic methods have been developed for the synthesis of indazole moieties. However to date much attention has been paid for the synthesis of thermodynamically stable 1*H*-indazoles as compared to its 2*H*-congeners.[10] Owing to the recently discovered potent bioactivity of 2*H*-indazole moieties, several synthetic groups developed numerous synthetic strategies. The most common synthetic strategies involved the use of Pd-catalyzed domino reaction of 2-halophenyl acetylenes with hydrazines, (3+2) cycloaddition of arynes and sydnones, Fe-catalyzed N-N bond formation of 2-azidophenyl ketoximes, reaction of 2-chloromethylarylzinc reagents and aryldiazonium salts, one-pot condensation−cadogan reductive cyclization from 2-nitrobenzaldehyde, Rh(III)-catalyzed C-H functionalization followed by cyclative capture, and Rh(III)-catalyzed [4+1]-annulation of azoxy compounds with alkynes or diazoesters.[11] In 2011, Lee et al. developed the CuI catalyzed multicomponent approach to 2*H*-indazole derivatives from 2-bromo benzaldehyde.[12] Recently, Sharghi et al. utilized Cu_2O nanoparticles for the indazole synthesis with limited substrate scope with no recyclability.[13] Most of the methods described above involved the consecutive formation of C-N and N-N bond for the synthesis of 2*H*-indazole derivatives represents one of the most efficient and atom-economical synthetic strategy in modern organic synthesis and green chemistry. Nonetheless, most of the synthetic methodologies have some drawbacks such as the use of expensive Pd and Rh catalyst with ligands, longer reaction time, harsh reaction conditions, decomposition of substrates during overheating, and problem of regioisomers which is problematic for industrial use due to high cost and waste disposal. To overcome these drawbacks, and to extend

the green and environment friendly alternative to the above mentioned synthetic sequences, great progresses have been made recently with new catalytic systems applying nanoparticles.

Recently with the discovery of inorganic nanoparticles with high surface-to-volume ratio and exposed surface features provide excellent catalytic activity with high product selectivity.[14] The different shapes of Cu_2O nanocrystals are widely pursued for the important organocatalytic, electrical conductivity, and photocatalytic properties.[15] According to the principle of green chemistry, the use of nanocatalysts looks to reduce energy and to optimize the use of the available resources, intending to become a sustainable strategy in chemical transformations. The nanoparticles increase the exposed surface area of the active component of the catalyst based of different shapes, thereby dramatically increasing the contact between reactants and catalyst which in turn mimicking the homogeneous catalysts by preserving the essential features of a heterogeneous catalysts. Recently, we have demonstrated the effectiveness of Cu_2O rhombic dodecahedra nanocrystals for the one-pot regioselective synthesis of 1,4-disubstituted triazoles and 3,5-disubstituted isoxazoles in green media.[16] Further in 2014, for the first time we have also performed the 1,3-dipolar cycloaddition to the synthesis of 1,2,3-triazoles in water by the use of superior Au nanocrystals.[17]

Regarding the wide array of applications of 2*H*-indazole derivatives as well as in view of the catalytic importance of Cu_2O rhombic dodecahedra for synthetic manipulation, we envisioned that the C-N, and N-N bond forming reaction for the 2*H*-indazole derivatives should be readily feasible. In continuation of our research to develop newer synthetic methodologies for the construction of bioactive heterocycles,[18] herein, we wish to report a novel Cu_2O rhombic dodecahedra catalyzed synthesis of 2*H*-indazole derivatives under mild conditions. This reaction proceeds very well under mild conditions and provides a good range of products in excellent yields with excellent regioselectivity. In addition, it avoids the requirement of a high temperature, and the reaction tolerates both electron-donating and electron-withdrawing substituents which make this protocol useful for the preparation of a series of 2*H*-indazole derivatives which can be further exploited in many applications. Further the synthesized compounds were evaluated for potential anti-cancer activity and live cell imaging.

Results and Discussion

At the onset of our study, the Cu_2O rhombic dodecahedra were synthesized in aqueous solutions following our already reported procedures.[16a] Exact amounts of $CuCl_2$ solution as precursor, SDS surfactant, NaOH solution, and NH_2OH•HCl as reducing agent were mixed at room temperature and aged for 1h for particle growth to yield the Cu_2O rhombic dodecahedra particle shapes. In order to evaluate the particle shape, the scanning electron micrograph (SEM) of the synthesized Cu_2O rhombic dodecahedra is shown in Figure 2 with an average particle size of ~ 340 nm along with size distribution histograms. The crystal structure and composition of the obtained sample were analyzed by X-ray diffraction which displays the XRD pattern of the rhombic dodecahedra with exceptional strong (110) and (220) peaks resulting from their {110} surface facets.

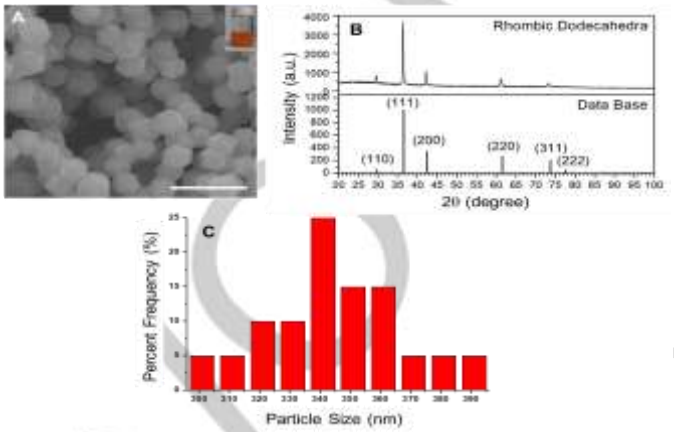

Figure 2. SEM images of (a) rhombic dodecahedral Cu_2O nanocrystals synthesized. The scale bars are equal to 1 µm. (b) XRD patterns of the synthesized Cu_2O rhombic dodecahedra. A standard diffraction pattern of Cu_2O is also given (JCPDS card no. 77-0199 for cuprite Cu_2O with a lattice constant a_o of 4.26 Å). Rhombic dodecahedra show enhanced (110) and (220) peaks as a result of their {110} faces. (c) Size distribution histograms of Cu_2O rhombic dodecahedra with average size of 340 ±28 nm.

In order to establish the optimum conditions, for our initial screening experiment, we choose the Cu_2O rhombic dodecahedra as catalyst based on our earlier results of synthesizing 1,4-triazoles and isoxazoles.[16a-b] The catalytic activity of Cu_2O rhombic dodecahedra was examined in a model reaction between 2-bromo benzaldehyde (**1a**), NaN_3 and aniline (**2a**) in refluxing EtOH as solvent for 10 h (Table 1, entry1). Disappointingly, only unreacted starting materials **1a** and **2a** were recovered from the reaction mixture. Unfortunately, the reaction did not afford any cyclized product using polar aprotic solvents such as CH_3CN, or THF (Table 1, entry 2, 3). By replacing the solvent system to DMF at 80 °C did not yield cyclized product **3** (Table 1, entry 4). By adding the N-containing ligand such as 1,10-phenanthroline in DMF at 80 °C for 10 h did not yield any cyclized product (Table 1, entry 5). However, by changing the solvent system to DMSO at 80 °C, the reaction was completed in 8 h with 60% yield (Table 1, entry 6). Surprisingly to our delight, it was found that the desired product **3a** was obtained in better yield when the reaction was performed in DMSO as solvent at 80 °C for 4 h using 1,10-phenanthroline as ligand (95% yield, Table 1, entry 7). Considering an improving yield of cyclized product **3**, increasing the catalyst loading upto 5 mol% did not lead to any further improvements (Table 1, entry 8).

Table 1. Optimization of nano Cu_2O rhombic dodecahedra catalyzed reaction of 2-bromo benzaldehyde **1a**, aniline **2a**, and NaN_3.[a]

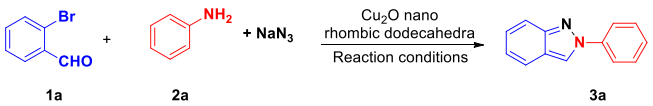

1a 2a 3a

Entry	Ligand	Solvent	Temperature	Time	Yield%[b]
1	-	EtOH	Reflux	10 h	0
2	-	CH_3CN	Reflux	10 h	0
3	-	THF	Reflux	10 h	0
4	-	DMF	80 °C	8h	0
5	1,10-Phen	DMF	80 °C	8h	0
6	-	DMSO	80 °C	8h	60%
7	1,10-Phen	DMSO	80 °C	4h	95%
8	1,10-Phen[c]	DMSO	80 °C	4h	95%

[a] Reaction was performed using **1a** (1 mmol), **2a** (1.2 mmol), NaN_3 (1.5 mmol). [b] Yield of the isolated product. [c] Reaction was carried out using 5 mol% of Cu(I) catalyst.

Finally, the optimized reaction conditions were found to be 2 mol% of nano Cu_2O rhombic dodecahedra (as the catalyst), DMSO (as a solvent), and 1,10-phenanthroline (as a ligand) at 80 °C for 4 h. With the optimized reaction conditions in hand, we next scrutinized the scope of the reaction using various aldehydes and amines. We tested various aromatic and aliphatic amines in the above reaction which yielded a series of 2*H*-indazoles as shown in Table 2. Interestingly, the reaction efficiency was not affected by the substituent groups on both substituted 2-bromo benzaldehyde **1** and aromatic amines **2**. In the case of aromatic amines having electron neutral and -donating groups, such as aniline, *p*-toluidine, *p*-anisidine, and *p*-isopropyl aniline excellent yields were obtained. The aromatic amines with electron withdrawing group such as 4-trifluoromethyl group obtained poor yields. The low yield could be probably due to the difficulty in formation of the imine intermediate by the reaction between aromatic aldehyde and aromatic amines. Similarly aliphatic amines or sterically hindered amine gave the corresponding of 2*H*-indazole derivatives **3** in good yields. All these reactions were performed under nitrogen atmosphere. The overall reaction time is typically 4-8 h as shown in Scheme 1.

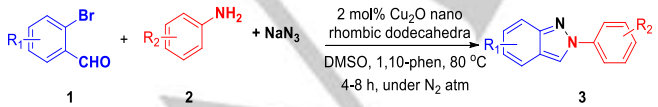

1 2 3

Scheme 1. Synthesis of nano Cu_2O rhombic dodecahedra catalyzed disubstituted 2*H*-indazoles **3**.

After completion of the reaction, the corresponding 2*H*-indazole derivatives were obtained with excellent yields followed by a simple work-up involving the filtration of the catalyst, removal, extraction, and solvent evaporation under reduced pressure. Finally the crude products were purified by column chromatography followed by spectroscopic characterization using analytical techniques. The results are summarized in Table 2. Recently, it has been realized that we need the broad and global transformation strategy for a sustainable chemistry which can contribute to sustainable development through efficient, economic and ecofriendly chemical synthetic methods. In view of this, Sheldon et al introduced the E-factor, or environmental impact factor which is to be measured by the waste produced in the process as opposed to the reaction.[19] Interestingly our green synthetic reaction conditions display lower E-factors (Table 2) for synthesizing many of the 2*H*-indazoles **3** which is consistent with the principles of atom economy.

Table 2. Substrate Scope of the Reaction and Physical Properties of Compound **3**.[a]

Entry	R_1	R_2	Yield[b]	H-bond donor	H-bond acceptor	c log P[c]	E-factor
3a	H	Ph	95	0	2	3.58	1.16
3b	H	4-$OCH_3C_6H_4$	92	0	3	3.75	1.13
3c	4-F	Ph	84	0	2	3.79	1.31
3d	H	4-$CH_3C_6H_4$	93	0	2	4.0	1.15
3e	4-F	4-$CH_3C_6H_4$	86	0	2	4.29	1.23
3f	H	$C_6H_5CH_2CH_2$	88	0	2	3.73	1.21
3g	4-OCH_3	Ph	92	0	3	3.70	1.07
3h	4-CH_3	Ph	95	0	2	4.07	1.08
3i	4-OCH_3	$C_6H_5CH_2CH_2$	90	0	3	3.86	1.03
3j	4-OCH_3	4-$CH_3C_6H_4$	94	0	3	3.70	0.99
3k	4-OCH_3	4-$OCH_3C_6H_4$	94	0	4	3.73	0.94
3l	4-CH_3	4-$CH_3C_6H_4$	95	0	2	4.57	1.03
3m	4-CH_3	4-$OCH_3C_6H_4$	95	0	3	4.25	0.98
3n	H	4-$CH(CH_3)_2C_6H_4$	94	0	2	5.0	1.15
3o	H	3,4-$(OCH_3)_2C_6H_3$	93	0	4	3.40	0.99
3p	4-CH_3	4-$CH(CH_3)_2C_6H_4$	94	0	2	5.5	0.85
3q	4-CH_3	3,4-$(OCH_3)_2C_6H_3$	94	0	4	3.90	0.93
3r	4-OCH_3	3,4-$(OCH_3)_2C_6H_3$	90	0	5	3.34	0.95
3s	H	4-$CF_3C_6H_4$	78	0	2	4.61	1.34

[a] Reaction conditions: 2-bromo benzaldehyde **1** (1 mmol), aniline **2** (1.2 mmol), NaN_3 (1.5 mmol), catalyst (2 mol%), 1,10-Phen (2 mol%) were reacted in DMSO (4 mL) at 80 °C, for 4-8 h. [b] Isolated yields. [c] Estimated c log P by ChemBioOffice 2010.

Furthermore, by utilizing the Lipinski's rule of five[20] we calculated the physicochemical properties of the synthesized library to compute the orally available drug properties. The rule states that, if the molecular weight is less than 500, the c log P value, which addresses bioavailability and delivery issues, is not more than 5, the hydrogen bond donors are not more than 5, the hydrogen bond acceptors and rotatable bonds are not more than 10 then that potential molecule can have drug-like physical properties. However, one Lipinski violation is allowed for the design of a potential molecule. Fortunately the predicted values

of drug-like properties for these 2*H*-indazole derivatives are within the accepted limits of Lipinski's rule of five as shown in Table 2.

Heterogeneous natures of Cu_2O rhombic dodecahedra were confirmed by performing the additional experiment. The hot filtration experiment was carried out using Cu_2O rhombic dodecahedra as the catalyst.[21] In the control experiment Cu_2O rhombic dodecahedra catalyzed heterocyclization was carried out at 80 °C for 2 h and then filtered at reaction temperature. The supernatant solution was gathered back into reaction vessel and continues the reaction for another 2 h which showed no catalytic activity. The filtered Cu_2O nanoparticles were redispersed in to fresh DMSO solution with fresh substrate catalyzed the new reaction with almost same activity (See supporting information figure 1). The filtration study clearly rules out any possible contribution of homogeneous catalysis by leached Cu(I) species in this cyclization reaction, so the observed catalytic activity is indeed due to heterogeneous catalysis.

A plausible mechanistic pathway for this heterocyclisation reaction is outlined in Scheme 2. The first step of the reaction involves the formation of imine intermediate A from the reaction of 2-bromo benzaldehyde **1** and aniline **2** followed by the activation of Br by the Cu(I) catalyst and azide ion to form the copper-azide complex **B**. The intermediate **B** then underwent electron reorganization followed by the removal of N_2 molecule and regeneration of Cu(I) catalyst to form the 2*H*-indazole derivative **3**.

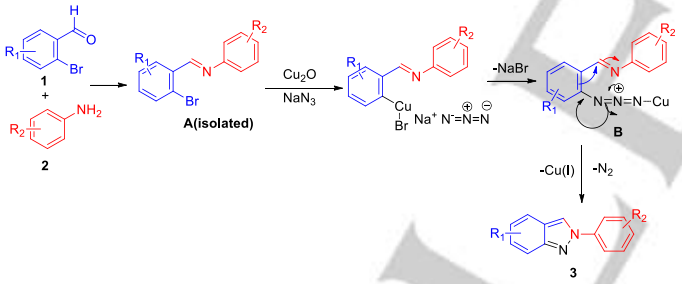

Scheme 2. Possible mechanism for heterocyclisation reaction to 2*H*-indazole derivatives **3**.

Further, the Cu_2O rhombic dodecahedra nanocatalyst could be effectively recycled and reused up to one consecutive catalytic cycle with a product yield of 80%.

Because potent anti-cancer activity has been reported for other indazole derivatives as evidenced from literature study,[22] we undertook the preliminary screening of all synthesized compounds **3a-s** for their cytotoxic activity against a panel of cancer cell lines such as human colon carcinoma (HCT-116), human lung carcinoma (A549), and human breast carcinoma (MDA-MB-468) by using MTT (3-(4,5-dimethylthiazol-2-yl)-2,5-diphenyltetrazolium bromide) assay. The results of this cytotoxicity assay expressed as IC_{50} values are summarized in Table 3. Commonly used wide spectrum anti-cancer drug cisplatin was used as a positive control. The colored formazan crystals formed after 48 h treatment of 2*H*-indazole compounds were measured at 570 nm. Among the nineteen different 2*H*-indazole derivatives screened, isopropyl substituted compound **3n** was found to have maximal cytotoxic effect in a concentration dependent manner, and was having the IC_{50} values of 26.1 µM, 37.1 µM and 25 µM in HCT-116, A549 and MDA-MB-468 cell lines respectively. We have chosen the effective IC_{50} concentration of 25 µM for further anti-cancer characterization studies with MDA-MB-468 cells.

Table 3. Half-maximum inhibitory concentration of synthesized 2*H*-indazole derivatives (IC_{50} values expressed in µM[a]).

Compound	A549[b]	MDA-MB-468[c]	HCT116[d]
3a	>100	97.7 ±1.5	96.2±1.5
3b	98.5±3.0	>100	95.7±2.3
3c	98.1 ±3.0	49.4±2.1	72.5±1.3
3d	45.6±2.0	32.5±1.7	44.2±3.5
3e	94.3±4.3	46.8±3.2	98±4.0
3f	>100	58.2±2.5	73.1±3.60
3g	>100	54.2±3.0	98.5±3.0
3h	>100	58.7±1.9	80.7±2.1
3i	37.2±0.6	30.2±3.1	50±2.6
3j	>100	>100	75.8±2.8
3k	50±2.5	35.6±0.8	67.1±3.0
3l	>100	>100	>100
3m	50.6±2.4	45.7±1.2	48.6±2.0
3n	37.1±2.0	25.0±2.5	26.1±3.4
3o	40.4±0.8	42.6±1.8	50.2±3.1
3p	29.0±3.8	29.4±1.2	40.5±2.1
3q	57.2±1.9	50.8±2.1	67.9±3.2
3r	35.9±2.0	39.6±0.8	37.6±1.8
3s	>100	>100	>100
DMSO	-	-	-
Cisplatin	7.5±3.0	5±2.0	5±2.1

[a] 50% inhibitory concentration values are an average of three individual experiments. [b] Lung cancer cells. [c] Breast cancer cells. [d] Colon cancer cells.

It is well established that cancer is a disease caused by the uncontrolled cell division where neoplastic cells undergo repeated mitosis. Mitosis is a stage of cell cycle where cell genome is duplicated and this is followed by cytokinesis. Usually the classical anti-cancer drugs effectively kill all the fast-proliferating cells by mediating unrepairable amount of DNA damage. These chromosomal alterations can be readily evaluated through the anti-mitotic study using *Allium cepa* root tip cells.

We clearly confirmed the presence of chromosomal aberrations and other nuclear abnormalities in compound **3n** with 25 µM concentration treated onion root tip cells comparable to that of cisplatin treated positive controls in Figure 3. Effectively when compared to the negative control, compound **3n** (25 µM) showed decrease in the mitotic index.

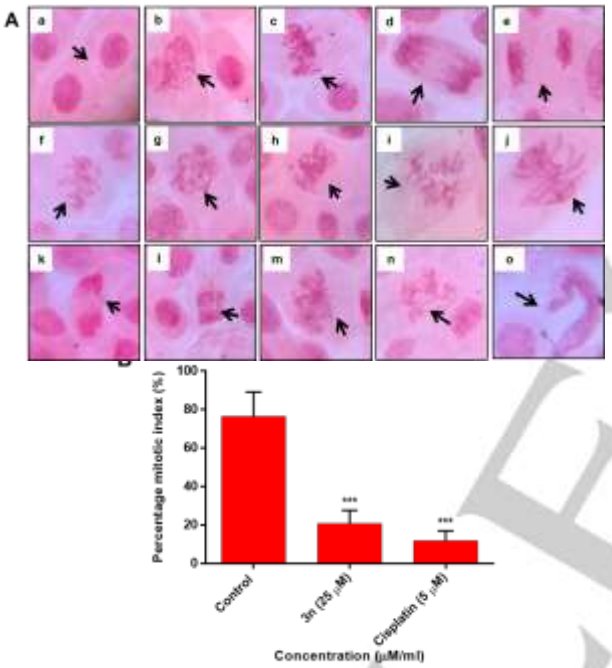

Figure 3. Effect of **3n** on inducing chromosomal aberration in *Allium cepa* root tip cells. A) (a-e) Control cells without compound **3n** showing normal mitotic phases - a) interphase, b) prophase, c) metaphase, d) anaphase and, e) telophase, f-o) cells showing aberrations upon treatment with **3n** (25 µM), f-g) sticky prophase, h) spindle disturbance at metaphase, i) c-mitosis and fragmented chromosomes at metaphase, j) sticky metaphase, k-n) bridges at anaphase, o) nuclear abnormalities. B) Histogram representing the percentage mitotic index versus drug concentration. The figures are representative of three independent experiments. Data is represented as Mean ± SD. *** P < 0.001 versus control.

To confirm the effect of compound **3n** on proliferation of MDA-MB-468 cells, a colony formation assay was carried out. The extent of cancer cells to produce colonies when plated at low densities is related with their proliferation potential, and the cytotoxic ability of test compound could correlate well with the inhibition of colony formation.[23] As shown in the Figure 4A, the MDA-MB-468 cells when treated with compound **3n** with 25 µM concentration showed a significant reduction in the number of colonies when compared to untreated control cells. The decrease in the colonies formed after treatment with compound **3n** can be correlated with the positive control cisplatin.

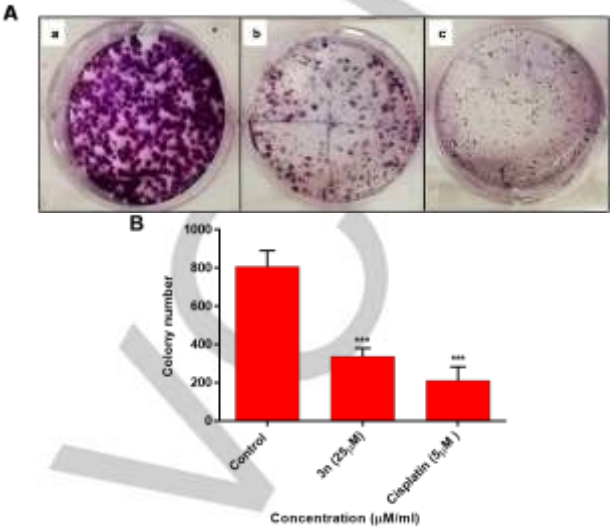

Figure 4. Effect of **3n** on colony formation ability of MDA-MB-468 cells *in vitro*. A) Represents the results of colony formation (a) Control, (b) MDA-MB-468 cells treated with **3n** (25 µM), (c) cells treated with cisplatin (5 µM). The number of colonies formed and the size of the colonies were significantly lesser upon treatment with 25 µM concentration of **3n** when compared to control. B) Histograms representing the number of colonies formed after 7 days of treatment. The figures are representative of three independent experiments. Data is represented as Mean ± SD. *** P < 0.05 versus control.

Apoptosis and necrosis are the major cell death principles, and among these apoptosis is the preferred choice for any cancer treatment. Apoptosis is a programmed cell death which efficiently removes the dysfunctional cells, and one hallmark property of cancer is ability of cancer cells to evade apoptosis.[24] Using the ethidium bromide (EtBr) and acridine orange (AO) double staining, we tested the ability of compound **3n** to induce apoptotic cell death in MDA-MB-468 cells. Through the fluorescent microscopic analysis, we showed the presence of cells bearing apoptotic nuclei after 24 h of treatment with compound **3n** at 25 µM concentration, which confirms the cell death through apoptosis. As shown in the Figure 5a, the untreated control cells appear uniformly green in colour and are marked as (L) whereas the MDA-MB-468 cells after 24 h of post treatment with compound **3n** at 25 µM concentration, showed both early apoptotic (EA) cells and late apoptotic (LA) cells (Figure 5b). In figure 5c, only late apoptotic (LA) cells were observed when treated with 5 µM concentration of cisplatin.

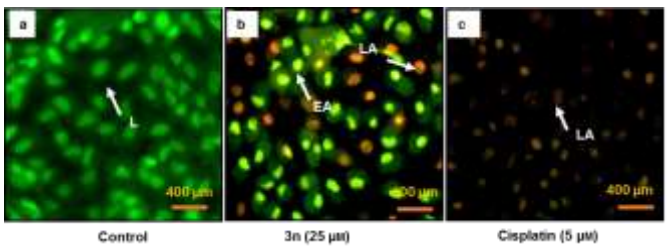

Figure 5. Effect of **3n** on inducing cellular apoptosis in MDA-MB-468 cells. The MDA-MB-468 cells were stained with Ethidium bromide and Acridine orange a) control cells (Live (L)), b) cells treated with 25 µM of **3n** showing cells of both early apoptotic (EA) and late apoptotic (LA) stages and c) cells treated with cisplatin (5 µM) showing late apoptotic (LA) cells. The figures are representative of three independent experiments.

By this assay, it is evident that the compound **3n** at 25 µM concentration promoted the apoptotic changes like nuclear fragmentation in MDA-MB-468 cells which can be co-relatable with the cisplatin induced changes. Thus, these results indicated the effectiveness of compound **3n** comparable to the commonly available anti-cancer drugs. These apoptotic related cell death was further evaluated by analyzing the disruption of mitochondrial membrane potential and caspase 3/7 activation.

Mitochondrial outer membrane permeabilization and disruption of mitochondrial transmembrane potential are frequently used as markers of apoptosis. Intact and functional mitochondria are the key indicator of cellular health, which can be assessed by monitoring the changes in mitochondrial membrane potential (MMP). During ATP synthesis by oxidative phosphorylation, the positively charged protons transferred across the inner membrane of mitochondria resulting in a net negative charged mitochondrial membrane potential ($\Delta\Psi m$). The MMP in healthy mitochondrial is strictly maintained at -180 mV. Tetramethylrhodamine ethyl ester perchlorate (TMRE) is a positively charged fluorescent dye which readily diffuse specifically into mitochondrial membrane due to the negative charge generated by MMP.[25] In this study, the treatment of MDA-MB-468 cells with the compound **3n** at 25 µM concentration caused the disruption in the mitochondrial membrane potential, and thus effectively decreased the fluorescence intensity when compared to control cells having uninterrupted bright fluorescence. Similar effect was observed in the cells treated with the positive control cisplatin at 5 µM concentration as depicted in Figure 6A.

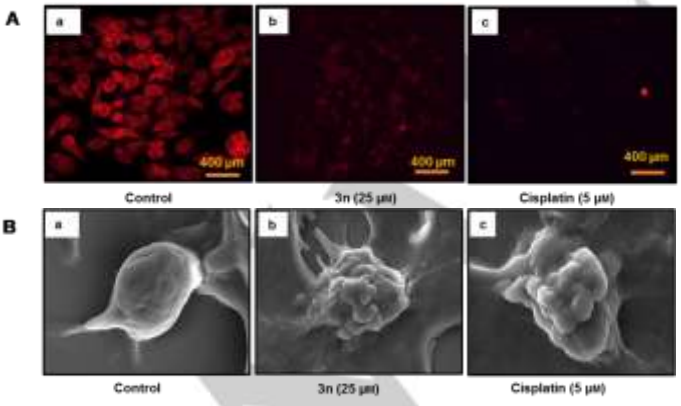

Figure 6. Effect of compound **3n** on mitochondrial membrane potential of MDA-MB-468 cells (A). The MDA-MB-468 cells were stained with TMRE to assess mitochondrial membrane potential a) control cells, b) cells treated with compound **3n** (25 µM), c) cells treated with cisplatin (5 µM). The figures are representative of three independent experiments. B) The effect of compound **3n** induced apoptotic morphology of MDA-MB-468 cells was determined by SEM analysis. a) Control, b) cells treated with compound **3n** (25 µM), c) cells treated with cisplatin (5 µM). The figures are representative of three independent experiments.

During the execution phase of apoptosis, certain changes occurs in the cell morphology which include cellular and nuclear contraction and membrane blebbing.[26] The activation of caspase 3 is said to be the necessary driving event for membrane blebbing.[27]

Caspases are cysteine-aspartic proteases which plays an important role in apoptosis. During apoptosis inactive initiator pro-caspases becomes rapidly cleaved and activated. Thus activated caspases in turn cleave a variety of downstream targets like effector caspases, nuclear, mitochondrial and plasma membrane proteins, thus ultimately leading to the programmed cell death.[28] In this study to confirm whether the cytotoxic effects of compound **3n** on MDA-MB-468 cells is caused indeed by apoptosis, effector terminal caspase-3/7 activity were checked by using the CellEvent™ Caspase 3/7 green detection reagent. This reagent contains a nucleic acid binding dye which gives bright green fluorescence upon binding to DNA after the release of inhibitory DEVD peptide portion. In apoptotic cells, the activated caspase-3/7 will cleave the DEVD peptide and allows the free dye to bind to the DNA and give fluorescence. As depicted in figure 7, the control cells with no bright green fluorescence were observed which indicated no sign of apoptosis. However, the cells treated with compound **3n** at 25 µM concentration showed bright green fluorescence indicating the activation of caspase-3/7 and apoptosis. Similar results were also observed in the breast cancer cells (MDA-MB-468) treated with 5 µM concentration of cisplatin.

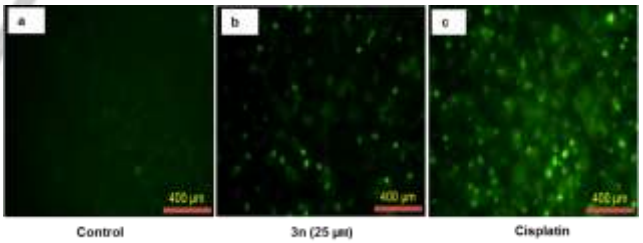

Figure 7. Effect of compound **3n** on activation of caspase 3&7 in MDA-MB-468 cells. The MDA-MB-468 cells were stained with CellEvent™ Caspase 3/7 Green Ready Probes™ Reagent (Invitrogen) to determine the activity of caspase 3&7. (a) Control cells, (b) cells treated with 25 µM concentration of **3n**, (c) cells treated with 5 µM concentration of cisplatin. The figures are representative of three independent experiments.

It is well known that the cellular migration and invasion play a crucial role in cancer cell metastasis. Pathogenesis and eventually the cancer related deaths are due to the spreading of the cancer cell from the primary site to other secondary sites during advanced stage of malignancy. This metastatic process includes the migration and invasion of the potent cancer cells to the adjacent tissues and organs through blood and lymphatic vessels.

In this regard, further in ascertaining the effect of compound **3n** on migration of MDA-MB-468 cells, we performed the in-vitro wound-healing assay.[29] The wounds made were almost of same size in each experimental cell group at 0 h as shown in Figure 8. Wound healing assay demonstrated that the compound **3n** at 25 μM concentrations could markedly inhibit the migration and wound closure capacity of MDA-MB-468 cells compared to that of control at 24 h. Similar effect was also observed in the cells treated with the positive control cisplatin at 5 μM concentrations. This assay illustrated the possible inhibitory effect of isopropyl substituted 2*H*-indazole compound **3n** on cancer metastasis which has to be evaluated further.

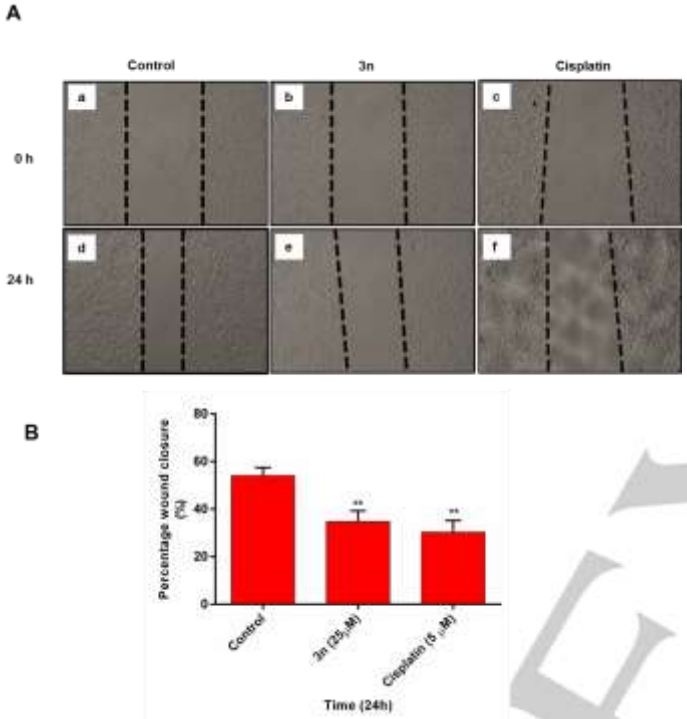

Figure 8. Effect of **3n** on inhibiting the migration of MDA-MB-468 cells. A) Representative images of **3n** inhibiting migration of MDA-MB-468 cells. The black dotted lines are representing the wound borders. The figures are representative of tee independent experiment; B) Histograms representing the percentage wound closure relative to 0 h of treatment. Data is represented as Mean ± SD. ** P < 0.05 versus control.

Overall these results indicated the effectiveness of isopropyl substituted 2*H*-indazole compound **3n** for anti-cancer treatment. MTT assays showed that compound **3n** inhibited the growth of A549, MDA-MB-468, and HCT116 cells in a time- and dose-dependent manner. The anti-proliferation effect of compound **3n** was further evidenced by the colony formation assay. Apoptosis mediated by the compound **3n** is through the mitochondrial pathway as mitochondrial potential loss was accomplished by caspases-3 and 7 activation. Compound **3n** also suppressed the migration and invasion of MDA-MB-468 cells. Resistance to cell death, unlimited replicative potential, clonal propagation, migration and tissue invasion are prominent features of cancer cells.[30] As malignant pathology is the outcome of these features and therefore targeting these crucial processes provides a perfect strategy to control cancers and its destruction. Our results indicated that 2*H*-indazole derivatives, specifically compound **3n** possessed significant anti-cancer activity and further development of such compound might be of interest to medicinal chemists.

Conclusions

In conclusion, we have developed Cu_2O rhombic dodecahedra catalyzed heteroannulation strategy for clean synthesis of 2*H*-indazoles with excellent yields. The salient features of this strategy include milder reaction conditions, inexpensive reagents, high-atom economy, and clean reaction profile in a single synthetic operation. These synthesized compounds were evaluated for their in vitro anti-cancer activity. Biological activity data indicated that compound with 4-isoprpoyl substituent on the 2*H*-indazole moiety showed significant inhibitory activity on the growth of A549, MDA-MB-468, and HCT116 cancer cells in a time- and dose-dependent manner and was evidenced further by induction of apoptosis, interrupting the colony formation abilities of cancer cells, blocking root-tip mitosis, and favoring death through extensive chromosomal aberrations. Further the compound suppressed the in vitro migration and invasion potential of cancer cells. These results suggested that with the inherent cytotoxic activity, these heterocyclic molecules might serve as interesting lead compounds, or for the development of new anti-cancer agents. Further medicinal characterization and applications of the 2*H*-indazole derivatives are currently under investigation in our laboratory.

Experimental Section

Chemistry

Unless otherwise indicated all common reagents and solvents were used as obtained from commercial suppliers without further purification. ^{1}H NMR (400 MHz, 600 MHz) and ^{13}C NMR (100 MHz, 150 MHz) were recorded on a Bruker DRX400 spectrometer. Chemical shifts are reported in ppm relative to the internal solvent peak. Coupling constants, J, are given in Hz. Multiplicities of peaks are given as: d (doublet), m (multiplet), s (singlet), and t (triplet). Mass spectra were recorded on a Perkin Elmer Calrus 600 GC-MS spectrometer. IR spectra were recorded on a Bomen DA8 3FTS spectrometer. Scanning electron microscopy (SEM) images of samples were obtained using a JEOL JSM-700F electron microscope. Powder X-ray diffraction (XRD) patterns were recorded on a Shimadzu XRD-6000 diffractometer with Cu Kα radiation. TLC plates were Merck silica gel 60 F_{254} on aluminum. Flash column chromatography was performed with silica gel (60−100 mesh). High resolution mass spectra (HRMS) were recorded in EI mode using JOEL JMS-HX 110 mass spectrometer.

General Procedure for the Synthesis of doubly substituted 2-aryl-2*H*-indazole 3. In a round bottomed flask under nitrogen atmosphere, a mixture of substituted 2-bromobenzaldehyde **1**(1.0 equiv), substituted aromatic amine **2** (1.2 equiv) was added to 4 mL solution of DMSO followed by the addition of NaN_3 (1.5 equiv). The reaction mixture was stirred for 5 minutes at room temperature condition followed by the addition Cu_2O rhombic dodecahedra catalyst (2 mol%) and 1,10-phen as ligand (2 mol%). The reaction mixture was stirred under heating condition at 80 ºC. The progress of the reaction was monitored by TLC. After completion, the reaction mixture was cooled to room temperature and was filtered to remove the catalyst, and extracted with ethyl acetate (10 mL, twice). The combined organic layer was dried over anhydrous $MgSO_4$. The combined filtrate was subjected to evaporation to obtain the

crude compound, which was purified over silica gel column (60–120 mesh) using 5-10% ethyl acetate in hexane as eluent to obtain the corresponding doubly substituted 2-aryl-2*H*-indazole **3** as the product.

2-Phenyl-2*H*-indazole (3a). Yield: 95%; white solid; ^{1}H NMR (400 MHz, $CDCl_3$) δ 8.29 (s, 1H), 7.80 (d, *J* = 8.6 Hz, 2H), 7.71 (d, *J* = 8.8 Hz, 1H), 7.60 (d, *J* = 8.6 Hz, 1H), 7.42 (t, *J* = 7.6 Hz, 2H), 7.29 (t, *J* = 7.1 Hz, 1H), 7.23 (t, *J* = 7.5 Hz, 1H) 7.02 (t, *J* = 7.16 Hz, 1H); ^{13}C NMR (100MHz, $CDCl_3$) δ 149.8,140.5, 129.6, 128.1, 127.9, 126.8, 122.8, 122.4, 121.0, 120.4, 117.6; MS (GC-MS) 194; HRMS (EI, m/z) calcd for $C_{13}H_{10}N_3$: m/z 194.0844; Found 194.0846.

2-(4-Methoxyphenyl)-2H-indazole (3b). Yield: 92%; white solid; ^{1}H NMR (300 MHz, $CDCl_3$) δ 8.33 (d, *J* = 1.0 Hz, 1H), 7.84-7.79 (m, 3H), 7.71 (dd, *J* = 8.4, 1.0 Hz, 1H), 7.37-7.34 (m, 1H), 7.15-7.10 (m, 1H), 7.04 (dd, *J* = 6.9, 2.0 Hz, 2H), 3.86 (s, 3H); ^{13}C NMR (75MHz, $CDCl_3$) δ 159.7, 149.8, 134.5, 126.9, 122.9, 122.8, 122.6, 120.8, 120.7, 118.1, 115.0, 56.0; MS (GC-MS) 224; HRMS (EI, m/z) calcd for $C_{14}H_{12}N_2O$: m/z 224.0950; Found 224.0951.

6-Fluoro-2-phenyl-2*H*-indazole (3c). Yield: 84%; pale brown solid; ^{1}H NMR (400 MHz, $CDCl_3$) δ 8.41 (s, 1H), 7.86 (d, *J* = 7.6 Hz, 2H), 7.69 (dd, *J* = 8.8, 5.2 Hz, 1H), 7.53 (t, J = 7.6 Hz, 2H), 7.43-7.35 (m, 2H), 6.93 (dt, J = 9.0, 0.8 Hz, 1H), 3.86 (s, 3H); ^{13}C NMR (100 MHz, $CDCl_3$) δ 162.2 (d, J_{CF} = 242 Hz, 1C), 149.5, 140.3, 129.6, 128.0, 122.3, 122.1. 120.8, 120.4, 114.5 (d, J_{CF} = 29 Hz, 1C), 101.1 (d, J_{CF} = 23.7 Hz, 1C); MS (GC-MS) 212; HRMS (EI, m/z) calcd for $C_{13}H_9FN_2$: m/z 212.0750; Found 212.0748.

2-(p-Tolyl)-2*H*-indazole (3d). Yield: 93%; white solid; ^{1}H NMR (400 MHz, $CDCl_3$) δ 8.36 (s, 1H), 7.78 (t, *J* = 8.6 Hz, 2H). 7.70 (d, *J* = 8.5 Hz, 1H), 7.33 (t, *J* = 8.4Hz, 3H), 7.11 (t, *J* = 8.0 Hz, 1H), 2.42 (s, 3H); ^{13}C NMR (100 MHz, $CDCl_3$) δ 149.6, 1.8.2, 137.9, 130.0, 126.6, 122.3, 120.9, 120.8, 120.4, 120.3, 117.8, 21.1; MS (GC-MS) 208; HRMS (EI, m/z) calcd for $C_{14}H_{12}N_2$: m/z 208.1000; Found 208.0996.

6-Fluoro-2-(p-tolyl)-2*H*-indazole (3e). Yield: 86%; pale brown solid; ^{1}H NMR (400 MHz, $CDCl_3$) δ 8.34 (d, *J* = 0.9 Hz, 1H), 7.72 (dd, *J* = 6.6, 2.0 Hz, 2H), 7.65 (d, *J* = 0.6 Hz, 1H), 7.30-7.23 (m, 2H), 6.90 (d, *J* = 2.0 Hz, 1H), 2.41 (s, 3H); ^{13}C NMR (100 MHz, $CDCl_3$) δ 162.8 (d, J_{CF} = 243 Hz, 1C), 149.6, 138.1, 129.9 (t, J_{CF} = 31.3 Hz, 1C), 122.2 (d, J_{CF} = 31.3 Hz, 1C), 120.7, 114.2 9 (t, J_{CF} = 28.5 Hz, 1C), 101.1 (d, J_{CF} = 23.76 Hz, 1C), 21.0; MS (GC-MS) 226; HRMS (EI, m/z) calcd for $C_{14}H_{11}FN_2$: m/z 226.0906; Found 226.0903.

2-Phenethyl-2*H*-indazole (3f). Yield: 88%; pale white solid; ^{1}H NMR (400 MHz, $CDCl_3$) δ 7.75 (dd, *J* = 8.6, 1.2 Hz, 1H), 7.69 (s, 1H), 7.59 (dd, *J* = 8.6, 1.0 Hz, 2H), 7.32-7.24 (m, 4H), 7.10 -7.05 (m, 3H), 4.42 (t, **J** = 7.6 Hz, 2H), 3.32 (t, *J* = 7.6 Hz, 2H); ^{13}C NMR (100 MHz, $CDCl_3$) δ 148.9, 137.7, 128.6, 128.5, 126.7, 125.8, 127.9, 121.5, 120.0, 117.3, 55.1, 37.0; MS (GC-MS) 222; HRMS (EI, m/z) calcd for $C_{15}H_{14}N_2$: m/z 222.1157; Found 222.1160.

6-Methoxy-2-phenyl-2*H*-indazole (3g). Yield: 92%; white solid; ^{1}H NMR (600 MHz, $CDCl_3$) δ 8.24 (s, 1H), 7.84 (dd, *J* = 7.6, 1.0 Hz, 2H) 7.65 (dd, *J* = 8.4, 1.0 Hz, 1H) 7.48 (dd, *J* = 7.4, 1.0 Hz, 1H), 7.36-7.34 (m, 1H), 7.01 (dd, *J* = 9.0, 2.1 Hz, 1H), 6.87 (d, *J* = 2.1 Hz, 1H), 3.83 (s, 3H); ^{13}C NMR (150 MHz, $CDCl_3$) δ 155.5, 146.7, 140.6, 129.5,127.5, 122.8, 122.0, 120.6, 119.3, 119.2, 96.3, 55.3; MS (GC-MS) 224; HRMS (EI, m/z) calcd for $C_{14}H_{12}N_2O$: m/z 224.0950; Found 224.0947.

6-Methyl-2-phenyl-2*H*-indazole (3h). Yield: 95%; white solid; ^{1}H NMR (600 MHz, $CDCl_3$) δ 8.31 (d, *J* = 8.8 Hz, 1H), 7.87 (t, *J* = 1.0 Hz, 1H), 7.85 (dd, *J* = 1.2, 0.8 Hz, 1H), 7.57 (d, *J* = 8.6 Hz, 1H), 7.51-7.48 (m, 3H), 7.36 (t, *J* = 7.3 Hz, 1H), 6.93 (dd, *J* = 8.6, 1.2 Hz, 1H), 2.45 (s, 3H); ^{13}C NMR (150 MHz, CDCl3) δ 150.4, 140.6, 1368, 129.5, 127.6, 125.5, 121.2, 120.8, 120.2, 119.9, 116.2, 22.3; MS (GC-MS) 208; HRMS (EI, m/z) calcd for $C_{14}H_{12}N_2$: m/z 208.1000; Found 208.1002.

6-Methoxy-2-phenethyl-2H-indazole (3i). Yield: 90%; off white solid; ^{1}H NMR (600 MHz, $CDCl_3$) δ 7.60 (d, *J* = 9.0 Hz, 1H), 7.55 (s, 1H), 7.26-7.24 (m, 2H), 7.21 (d, *J* = 7.3 Hz, 1H) 7.08 (dd, *J* = 8.3, 1.5 Hz, 2H), 6.97 (dd, *J* = 9.0, 2.4 Hz, 1H), 6.80 (d, *J* = 2.4 Hz, 1H), 4.55 (t, *J* = 7.4 Hz, 2H), 3.79 (s, 3H), 3.27 (t, *J* = 7.4 Hz, 2H); ^{13}C NMR (150 MHz, $CDCl_3$) δ 154.9, 145.7, 137.9, 128.7, 128.6, 126.7, 122.04, 121.4, 120.5, 118.7, 96.6, 55.3, 54.9, 37.1; MS (GC-MS) 252; HRMS (EI, m/z) calcd for $C_{16}H_{16}N_2O$: m/z 252.1263; Found 252.1269.

6-Methoxy-2-(p-tolyl)-2*H*-indazole (3j). Yield: 94%; pale white solid; ^{1}H NMR (600 MHz, $CDCl_3$) δ 8.17 (s,1H), 7.70 (d, *J* = 8.3 Hz, 2H), 7.66 (dd, *J* = 9.0, 0.7 Hz, 1H), 7.25 (dd, *J* = 8.3, 0.7 Hz, 2H), 7.01 (dt, *J* =7.3, 2.3 Hz, 1H), 6.84 (d, *J* = 2.3 Hz, 1H), 3.81 (s, 3H), 2.38 (s, 3H); ^{13}C NMR (150 MHz, $CDCl_3$) δ 155.4,146.5, 138.3, 137.4, 129.9, 122.6, 121.7, 128.4, 119.2, 119.1, 96.3, 55.3, 20.9; MS (GC-MS) 252; HRMS (EI, m/z) calcd for $C_{15}H_{14}N_2O$: m/z 238.1106; Found 238.1115.

6-Methoxy-2-(4-methoxyphenyl)-2*H*-indazole (3k). Yield: 94%; pale white solid; ^{1}H NMR (600 MHz, $CDCl_3$) δ 8.12 (s, 1H), 7.72 (dd, *J* = 6.9, 2.2 Hz, 2H), 7.65 (d, *J* = 9.2 Hz, 1H), 6.99 (dd, *J* = 9.2, 2.2 Hz, 1H), 6.85(d, *J* = 2.2 Hz, 1H), 6.97 (dd, *J* = 6.9, 2.2 Hz, 2H), 3.82 (s, 3H), 3.81 (s, 3H); ^{13}C NMR (150 MHz, $CDCl_3$) δ 158.9, 155.4, 146.4, 134.2, 122.6, 121.9, 121.5, 119.2, 119.1, 114.5, 96.3, 55.5, 55.3; MS (GC-MS) 254; HRMS (EI, m/z) calcd for $C_{15}H_{14}N_2O_2$: m/z 254.1054; Found 254.1057.

6-Methyl-2-(p-tolyl)-2*H*-indazole (3l). Yield: 95%; pale yellow solid; ^{1}H NMR (600 MHz, $CDCl_3$) δ 8.26 (s, 1H), 7.72 (d, *J* = 8.0 Hz, 2H), 7.55 (d, *J* = 8.3 Hz, 2H), 7.52 (s, 1H), 7.26 (dd, *J* = 8.0, 0.7 Hz, 2H), 6.93 (d, *J* = 8.3 Hz, 1H), 2.45 (s, 3H), 2.39 (s, 3H); ^{13}C NMR (150 MHz, $CDCl_3$) δ 150.2, 138.3, 137.5, 136.5, 129.9, 125.2, 121.0, 120.6, 120.0,119.8, 116.1, 22.2, 20.9; MS (GC-MS) 222; HRMS (EI, m/z) calcd for $C_{15}H_{14}N_2$: m/z 222.1157; Found 222.1154.

2-(4-Methoxyphenyl)-6-methyl-2*H*-indazole (3m). Yield: 95%; off white solid; ^{1}H NMR (600 MHz, $CDCl_3$) δ 8.19 (d, *J* = 1.0 Hz, 1H), 7.74 (dd, *J* = 6.9, 2.2 Hz, 2H), 7.54 (d, *J* = 8.6 Hz, 1H), 7.51(dd, *J* = 2.2, 0.9Hz, 1H) 6.97(dd, *J* = 6.9, 2.2Hz, 2H), 6.92 (dd, *J* = 8.6, 1.0 Hz, 1H), 3.82 (s, 3H), 2.45 (s, 3H); ^{13}C NMR (150 MHz, $CDCl_3$) δ 159.1, 150.2, 136.4, 134.1, 125.1, 122.2, 121.0,120.0, 119.7,116.0, 114.5, 55.5, 22.2; MS (GC-MS) 238; HRMS (EI, m/z) calcd for $C_{15}H_{14}N_2O$: m/z 238.1106; Found 238.1105.

2-(4-Isopropylphenyl)-2*H*-indazole (3n). Yield: 94%; off white solid; ^{1}H NMR (600 MHz, $CDCl_3$) δ 8.34 (d, *J* = 1.0 Hz, 1H), 7.80-7.77 (m, 3H), 7.68 (dd, *J* = 8.5, 0.9 Hz, 1H), 7.35 (dd, *J* = 1.7, 2.0 Hz, 2H), 7.31-7.29 (m, 2H), 7.10-7.08 (m, 1H), 2.97 (quart, *J* = 7.8 Hz, 1H), 1.29 (s, 3H), 1.27 (s, 3H); ^{13}C NMR (150 MHz, $CDCl_3$) δ 149.6,148.8, 138.5, 127.5,126.6,122.7, 122.3, 120.9, 120.3, 120.3, 117.9, 33.7, 23.9; MS (GC-MS) 236; HRMS (EI, m/z) calcd for $C_{16}H_{16}N_2$: m/z 236.1313; Found 236.1312.

2-(3,4-dimethoxyphenyl)-2*H*-indazole (3o). Yield: 93%; white solid; ^{1}H NMR (600 MHz, $CDCl_3$) δ 8.22 (s, 1H), 7.74 (d, *J* = 8.8, Hz, 1H), 7.60 (d,

J = 8.5 Hz, 1H), 7.47 (d, *J* = 2.3 Hz, 1H), 7.27-7.24 (m, 1H), 7.21 (dt, *J* = 8.5, 0.7 Hz, 1H), 7.04 (dd, *J* = 7.5, 0.8 Hz, 1H), 6.82 (d, *J* = 8.8 Hz, 1H); ^{13}C NMR (150 MHz, $CDCl_3$) δ 149.5, 149.3, 148.7, 134.1,126.4, 122.5, 122.1, 120.3, 120.1, 117.5, 112.4, 111.1, 105.3, 56.0, 55.9; MS (GC-MS) 254; HRMS (EI, m/z) calcd for $C_{15}H_{14}N_2O_2$: m/z 254.1055; Found 254.1060.

2-(4-Isopropylphenyl)-6-methoxy-2*H*-indazole (3p). Yield: 94%; white solid; ^{1}H NMR (600 MHz, $CDCl_3$) δ 8.20 (d, *J* = 0.7 Hz, 1H), 7.76 (d, *J* = 8.5 Hz, 2H), 7.69 (d, *J* = 9.0 Hz, 1H), 7.34 (d, *J* = 8.5 Hz, 2H), 7.04 (td, *J* = 9.0, 1.5 Hz, 1H), 6.87 (d, *J* = 2.0 Hz, 1H), 3.83 (s, 3H), 2.97 (m, 1H), 1.30 (d, *J* = 1.8 Hz, 3H), 1.29 (d, *J* = 1.8 Hz, 3H); ^{13}C NMR (150 MHz, $CDCl_3$) δ 155.4, 148.4, 146.5, 138.5, 127.4, 122.6, 121.7, 120.5, 119.3, 119.1, 96.3, 55.2, 33.7, 23.8; MS (GC-MS) 266; HRMS (EI, m/z) calcd for $C_{17}H_{18}N_2O$: m/z 266.1419; Found 266.1418.

2-(3,4-dimethoxyphenyl)-6-methyl-2*H*-indazole (3q). Yield: 94%; white solid; ^{1}H NMR (600 MHz, $CDCl_3$) δ 8.22 (s, 1H), 7.54 (d, *J* = 8.5 Hz, 2H), 7.49 (dd, *J* = 9.0, 1.0 Hz, 1H), 7.26-7.24 (m, 1H), 6.92 (d, *J* = 8.5 Hz, 1H), 6.90 (d, *J* = 8.5 Hz, 1H), 3.96 (s, 3H), 3.90 (s, 3H), 2.44 (s, 3H); ^{13}C NMR (150 MHz, $CDCl_3$) δ 150.1. 149.5, 148.6, 136.5, 134.3, 125.2, 120.9, 120.2, 119.7, 115.9, 112.4, 111.1, 105.3, 56.1, 56.0, 22.2; MS (GC-MS) 268; HRMS (EI, m/z) calcd for $C_{16}H_{16}N_2O_2$: m/z 268.1212; Found 268.1209.

2-(3,4-dimethoxyphenyl)-6-methoxy-2*H*-indazole (3r). Yield: 90%; white solid; ^{1}H NMR (600 MHz, $CDCl_3$) δ 8.17 (d, *J* = 0.9 Hz, 1H), 7.65 (d, *J* = 9.2 Hz, 1H), 7.48 (d, *J* = 2.5 Hz, 1H), 7.25 (dd, *J* = 8.5, 2.5 Hz, 1H), 7.00 (dd, *J* = 9.2, 2.2 Hz, 1H), 6.92 (d, *J* = 8.5 Hz, 1H), 6.87 (d, *J* = 2.2 Hz, 1H), 3.97 (s, 3H), 3.91 (s, 3H), 3.83 (s, 3H); ^{13}C NMR (150 MHz, $CDCl_3$) δ 155.4, 149.7, 148.6, 146.5, 134.5, 122.7, 121.7. 119.4, 119.1, 112.3, 111.2, 105.3, 96.3, 56.2, 55.3; MS (GC-MS) 284; HRMS (EI, m/z) calcd for $C_{16}H_{16}N_2O_3$: m/z 284.1161; Found 284.1162.

2-(4-(Trifluoromethyl)phenyl)-2*H*-indazole (3s). Yield: 83%; yellow solid; ^{1}H NMR (400 MHz, $CDCl_3$) δ 8.47 (s, 1H), 8.06 (d, *J* = 8.4 Hz, 2H), 7.78 (t, *J* = 8.4 Hz, 3H), 7.71(d, *J* = 8.5 Hz, 1H), 7.34 (t, *J* = 7.0 Hz, 1H), 7.13 (t, *J* = 8.1 Hz, 1H); ^{13}C NMR (100MHz, $CDCl_3$) δ 150.2, 127.5, 126.9, 126.9, 126.8, 126.8, 123.0, 123.0, 120.7, 120.4,118.0; MS (GC-MS) 262.

Biology

Chemicals and reagents

3-(4,5-dimethylthiazol-2-yl)-2,5-diphenyltetrazolium bromide (MTT), ethidium bromide, acridine orange, Acetocaramine, crystal violet, glacial acetic acid methanol were purchased from Himedia. Tetramethylrhodamine ethyl ester perchlorate (TMRE) and cisplatin were obtained from Sigma Aldrich. CellEvent™ Caspase 3/7 Green Ready Probes™ Reagent was obtained from Invitrogen.

Cell lines and cell culture conditions

Human colon cancer cell line (HCT-116), human lung cancer cell line (A549), human breast cancer cell line (MDA-MB-468) were obtained from National centre for cell sciences (NCCS), Pune, India. The cells were maintained in Dulbecco's modified Eagle's Medium (DMEM, Himedia) supplemented with 10% fetal bovine serum (FBS, Himedia), 100 µg/mL streptomycin, and 100 U/mL penicillin (Himedia) in a humidified incubator under 5% CO_2 and 20% O_2 at 37 °C.

Cell viability assay

The effect of novel 2*H*-indazoles on the cell viability of the A549, HCT-116 and MDA-MB-468 cell lines was analysed by 3-(4,5-dimethylthiazol-2-yl)-2,5-diphenyltetrazolium bromide (MTT) assay with slight modifications as reported previously.[31] Briefly, 1×10^4 cells were seeded in 96 well plates and after the cells reached about 70%-80% confluency, the cells were treated with different concentrations of 2*H*-indazoles for 24 h. Cisplatin served as positive control and DMSO was the untreated vehicle control. In all the treatments, final concentration of DMSO did not exceed more than 0.25 % in the medium. After the treatment, MTT (5mg/ml in 1X Phosphate Buffered Saline (1XPBS) was added into the each well and incubated for 4 h. At the end of the incubation DMSO was added and the purple color formation was analyzed by using ELISA plate reader at 570 nM (BioTek-ELx800). The IC_{50} values were calculated from the graphs by plotting percentage cell viability against drug concentration. All the experiments were made in triplicates.

Allium cepa root tip assay

Antimitotic activity of compound **3n** was tested by using Allium cepa root tip cells with few modifications in the previously reported protocol.[32] Onion bulbs of good quality were taken and skin was peeled off. The onion bulbs were placed on distilled water and allowed to develop the roots. After the root formation the bulbs were transferred to the tubes containing compound **3n** and incubated for 24 h. Simultaneously the control bulbs were maintained in distilled water as such without treating with the drug. Cisplatin (5 µM) is used as a positive control. The root tips of around 2-3 mm were cut and fixed with Carnoy's fixative and hydrolysed in 1N HCl for 15min. The root tips were stained with acetocarmine solution and squash was prepared. The images were taken under microscope (OLYMPUS-CKX41SF). The mitotic index was calculated using following formula.

Mitotic index = Number of dividing cells/ total number of cells×100

Treatment groups	Total cells counted	Cells in Mitotic phase				Total mitotic cells	% Mitotic index	No of aberrant mitotic cells	% of aberrant mitotic cells
		Prophase	Metaphase	Anaphase	Telophase				
Control	490	96	116	78	25	315	64.2857	0	0
25 µm	300	29	11	7	6	51	13.0769	51	100
Cisplatin	419	17	5	4	0	26	6.2052	26	100

Colony formation assay:

To check the effect of compound **3n** on survival and proliferation of MDA-MB-468 cell line, colony formation assay was performed.[33] Briefly 1×10^3 cells per well in 6-well plates and after reaching 70%-80% confluency, the cells were treated with compound **3n** (25 μM) for 24 h, whereas cisplatin (5 μM) was used as positive control. The untreated cells were served as control. Then the cells were incubated further for 14-20 days to form the colonies. Formed colonies were fixed with 4% paraformaldehyde, and then stained with 0.5% of crystal violet for 15 min. The number of colonies produced was counted manually.

Ethidium bromide (EtBr) and Acridine orange (AO) double staining assay:

To analyze the effect of **3n** on inducing apoptotic changes in MDA-MB-468 cells, EtBr and AO double staining assay was performed with slight modifications as reported before.[34] The MDA-MB-468 cells were grown on coverslips and then treated with compound **3n** (25 μM) for 24 h. Control cells were maintained without adding compound **3n**, whereas cisplatin (5 μM) was used as the positive control. After the incubation, to the cells staining solution consisting of acridine orange (100 μg/ml) and ethidium bromide (100 μg/ml) was added and incubated for 5 min in dark. Then the coverslips were examined for the staining pattern under fluorescent microscope (WEXEX OPTIK-FM 300).

Mitochondrial transmembrane potential (ΔΨm) analysis:

To analyze the mitochondrial inner membrane depolarization caused by compound **3n**, a fluorescent dye Tetramethylrhodamine ethyl ester perchlorate (TMRE) staining was performed with slight modifications in the previously reported protocol.[35] The MDA-MB-468 cells were grown on coverslips and incubated until they reach confluency. Then the cells were treated with compound **3n** (25 μM) for 24 h. Control cells were maintained untreated and Cisplatin (5 μM) was used as positive control. To the coverslips staining solution consisting of TMRE (150 nM) was added and incubated in dark for 20 min in dark. Then the coverslips were carefully placed on to a clean microscopic slide and cells were examined for their mitochondrial membrane depolarisation under fluorescent microscope (WEXEX OPTIK-FM 300).

Apoptotic morphological analysis by SEM:

To check the effect of compound **3n** on inducing apoptosis, the apoptosis morphology analysis is performed by Scanning electron microscope (SEM). Briefly MDA-MB-468 cells were seeded at a minimal density on coverslips in multi well culture plates and allowed to reach 70-80% confluency before treating with compound **3n** (25 μM), or cisplatin (5 μM) for 24 h. The control cells were left untreated. After incubation cells were then washed trice with 1X PBS, and fixed for 2h with 2.5% glutaraldehyde at 4ºC. Dehydration was performed with gradients of 30, 50, 70, 80, 90, 96 and 100% ethanol, at 15 min intervals and left for drying for 48 h. MDA-MB-468 cell surface was coated with gold spray and examined by SEM (ZEISS-EVO 18).

Detection of Caspase 3/7 activity:

Activation of caspase 3 and 7 was analysed using CellEvent™ Caspase 3/7 Green Ready Probes™ Reagent (Invitrogen). According to manufacturer's protocol, 1×10^5 MDA-MB-468 cells were seeded on glass coverslips placed in a six well plate and treated with compound of **3n** (25 μM). The control cells were maintained without addition of compound **3n** and incubated for 24 h. After the treatment each well was loaded with 2 drops of CellEvent™ Caspase 3/7 Green Ready Probes™ Reagent and incubated for 30 min at 37°C. Then the coverslips were removed from the wells and caspase 3/7 positive cells were analysed on a fluorescence microscope (WEXEX OPTIK-FM 300).

***In vitro* Wound healing migration assay:**

To analyse the effect of compound **3n** on migration of MDA-MB-468 was performed by using wound healing assay.[36] Cells were seeded at a density of 3×10^5 cells per well in a 6-well plate and incubated 24 h. A single wound was made on the plates by using a 200 µl sterile pipette tip. The plates were washed with sterile 1X PBS to remove the cell debris and treated with compound **3n** (25 μM) for 24 h. Control cells were maintained untreated and Cisplatin (5 μM) was used as positive control. The images were taken at 0 h and 24 h intervals after the drug additions using inverted microscope (MAGNUS-10J617). The area of the wound was measured by using Image J software. The migration of the cells into the wound area is represented as the percentage of wound closure relative to 0 h. The percentage wound closure was calculated by using the following formula.

% Wound closure = (original scratch width - new scratch width)/original scratch width ×100%).

Statistical analysis

The values obtained in the experiments are expressed as the mean ± standard deviation (SD) and were analyzed by one-way analysis of variance (ANOVA) where necessary with a post Dunnett's multiple comparisons test. A P-value of less than 0.05 was considered statistically significant

Acknowledgements

The authors thank the Chancellor and Vice Chancellor of VIT University for providing opportunity to carry out this study. Further the authors RLP, VM and KC wish to thank the management of this university for providing seed money as research grant. Kaushik Chanda thanks CSIR-Govt. of India for funding through Grant no 01(2913)/17/EMR-II. Thanks are also

to Central instrumentation facility VIT University for recording the spectra.

Keywords: 2*H*-Indazole • Cu_2O rhombic dodecahedra • anti-cancer activity • apoptosis • cisplatin • heterocyclization.

References:

[1] a) D. M. D'Souza, T. J. J. Müller, *Chem. Soc. Rev*. **2007**, *36*, 1095-1108; b) F. Hu, M. Szostak, *Adv. Synth. Catal*. **2015**, *357*, 2583-2614.

[2] L. A. Clutterbuck, C. G. Posada, C. Visintin, D. R. Riddal, B. Lancaster, P. J. Gane, J. Garthwaite, D. L. Selwood, *J. Med. Chem*. **2009**, *52*, 2694-2707.

[3] S. Qian, J. Cao, Y. Yan, M. Sun, H. Zhu, Y. Hu, Q. He, B. Yang, *Mol. Cell. Biochem*. **2010**, *345*, 13-21.

[4] W. Han, J. C. Pelletier, C. N. Hodge, *Bioorg. Med. Chem. Lett.* **1998**, *8*, 3615-3620.

[5] X. Li, S. Chu, V. a. Feher, M. Khalili, Z. Nie, S. Margosiak, V. Nikulin, J. Levin, K. G. Sparankle, M. E. Fedder, R. Almassy, K. Appelt, K. M. Yager, *J. Med. Chem*. **2003**, *46*, 5663-5673.

[6] M. D. Angelis, F. Stossi, K. A. Carlson, B. S. Katzenellenbogen, J. A. Katzenellenbogen, *J. Med. Chem*. **2005**, *48*, 1132-1144.

[7] J. Catalán, J. C. del Valle, R. M. Claramunt, G. Boyer, J. Laynez, J. Gómez, P. Jiménez, F. Tomás, J. Elguero, *J. Phys. Chem*. **1994**, *98*, 10606-10610.

[8] a) C. K. Chung, P. G. Bulger, B. Kosjek, K. M. Belyk, N. Rivera, M. E. Scott, G. R. Hunphery, J. Limanto, D. C. Bachert, K. M. Emerson, *Org. Process Res. Dev*. **2014**, *18*, 215-227; b) Y. Jia, J. Zhang, J. Feng, F. Xu, H. Pan, W. Xu, *Chem. Biol. Drug Des*. **2014**, *83*, 306-316; c) S. Tomassi, J. Lategahn, J. Engel, M. Keul, H. L. Tumbrink, J. Ketzer, T. Mühlenberg, M. Baumann, C. Schultz-Fademrecht, S. Bauer, D. Rauh, *J. Med. Chem*. **2017**, *60*, 2361−2372.

[9] P. Nareddy, F. Jordan, M. Szostak, *ACS Catal*. **2017**, *7*, 5721-5745.

[10] J. J. Song, N. K. Yee, *Org. Lett*. **2000**, *2*, 519-522.

[11] a) N. Halland, M. Nazaré, O. R'kyek, J. Alonso, M. Urmann, A. Lindenschmidt, *Angew. Chem. Int. Ed*. **2009**, *48*, 6879-6885; b) C. Wu, Y. Fang, R. C. Larock, F. Shi, *Org. Lett.* **2010**, *12*, 2234-2237; c) B. J. Stokes, C. V. Vogel, L. K. Urnezis, M. Pan, T. G. Driver, *Org. Lett*. **2010**,*12*, 2884-2887; d) B. Haag, Z. Peng, P. Knochel, *Org. Lett.* **2009**, *11*, 4270-4273; e) Y. Lian, R. G. Bergman, L. D. Lavis, J. A. Ellman, *J. Am. Chem. Soc*. **2013**, *135*, 7122-7125; f) N. E. Genung, L. Wei, G. E. Aspnes, *Org. Lett.* **2014**, *16*, 3114-3117; g) Z. Long, Y. Yang, J. You, *Org. Lett*. **2017**, *19*, 2781-2784. (h) Z. Long, Z. Wang, D. Zhou, D. Wan, J. You, *Org. Lett*. **2017**, *19*, 2777-2780.

[12] M. R. Kumar, A. Park, M. Park, S. Lee, *Org. Lett*. **2011**, *13*, 3542-3545.

[13] H. Sharghi, M. Aberi, *Synlett*, **2014**, *25*, 1111-1115.

[14] a) I. Lee, F. Delbecq, R. Morales, M. A. Albiter, F. Zaera, *Nat. Mater.* **2009**, *8*, 132–138; b) Y. Wu, S. Cai, D. Wang, W. He, Y. Li, *J. Am. Chem. Soc*. **2012**, *134*, 8975–8951.

[15] a) M. Li, X. Xing, Z. Ma, J. Lv, P. Fu, Z. Li, *ACS Sustainable Chem. Eng*. **2018**, *6*, 5495−5503; b) C. S. Tan, S. C. Hsu, W. H. Ke, L. J. Chen, M. H. Huang, *Nano Lett*. **2015**, *15*, 2155–2160; c) Y. Su, H. Li, H. Ma, J. Robertson, A. Nathan. *ACS Appl. Mater. Interfaces.* **2017**,9, 8100−8106.

[16] a) K. Chanda, S. Rej, M. H. Huang, *Chem. Eur. J.* **2013**, *19*, 16036–16043; b) K. Chanda, S. Rej, M. H. Huang, *Nanoscale*, **2013,** *5*, 12491-12501; c) Y. H. Tsai, K. Chanda, Y. T. Chu, C.-Y. Chiu, M. H. Huang, *Nanoscale*, **2014**, 6, 8704-8709.

[17] S. Rej, K. Chanda, C.-Y. Chiu, M. H. Huang, *Chem. Eur. J,* **2014**, *20*, 15991-15997.

[18] a) B. Maiti, K. Chanda, *RSC. Adv*. **2016**, *6*, 50384-50413; b) R. N. Rao, B. Maiti, K. Chanda, *ACS Comb. Sci.* **2017**, *19*, 199-228; c) R. N. Rao, M. M. Balamurali, B. Maiti, R. Thakuria, K. Chanda, *ACS. Comb. Sci.* **2018**, *20,* 164-171; d) R. D. Padmaja, K. Chanda, *Org. Process Res. Dev*. **2018**, *22*, 457-466; e) R. D. Padmaja, C. V. Devi; N. Mukku, K.Chanda, B. Maiti, *ACS Omega*, **2018**, *3*, 4583–4590.

[19] a) R. A. Sheldon, *Green Chem*. **2007**, *9*, 1273-1283; b) R. A. Sheldon *Chem. Soc. Rev*. **2012**, *41*, 1437-1451.

[20] a) C. A. Lipinski, F. Lombardo, B. W. Dominay, P. J. Feeney, *Adv. Drug Delivery Rev*. **1997**, *23*, 3-25; b) C. A. Lipinski, F. Lombardo, B. W. Dominy, P. J. Feeney, *Adv. Drug Delivery Rev.* **2001**, *46*, 3-26; c) D. F. Veber, S. R. Johnson, H.-Y. Cheng, B. R. Smith, K. W. Ward, K. D. Kopple, *J. Med. Chem.* **2002**, *45*, 2615-2623.

[21] H. E. B. Lempers, R A. Sheldon, *J. Catal*. **1998**, *175*, 62-69.

[22] N. M. Y. Elsayed, D. A. Abou El Ella, R. A. T. Serya, M. F. Tolba, R. K. Shalaby, A. M. Abouzid, *Med. Chem. Commun*. **2016**, *7*, 881-899.

[23] S. Horibata, T. V. Vo, V. Subramanian, P. R. Thompson, S. A. Coonrod, *J. Visualized Exp*. **2015**, e52727.

[24] J. M. Brown, L. D. Attardi, *Nat. Rev. Cancer*. **2005**, *5*, 231-237.

[25] S. Sakamuru, M. S. Attene-Ramos, M. Xia. Mitochondrial Membrane Potential Assay, *Vol. 1473* (Eds.: In: Zhu H., Xia M) High-Throughput Screening Assays in Toxicology. Methods in Molecular Biology Humana Press, New York, NY. **2016**, Pp. 17-22,

[26] M. L. Coleman, E. A. Sahai, M. Yeo, M. Bosch, A. Dewar, M. F. Olson, *Nat Cell Biol*. **2001**, *3*, 339-45.

[27] Y. Zhang, X. Chen, C. Gueydan, J. Han, *Cell Res*. **2018**, *28*, 9–21.

[28] Y. Shi, Protein *Science*, **2004**, *13*, 1979–1987.

[29] R. Riahi, Y. Yang, D. D. Zhang, P. K. Wong, *J. Lab. Autom*. **2012**, *17*, 59–65.

[30] D. Hanahan, R. A. Weinberg, *Cell*, **2011**, *144*, 646–674.

[31] T. Mosmann, *J Immunol Methods*. **1983**, *65*, 55-63.

[32] S. Anjana, J. E. Thoppil, *Int. J. Res. Dev. Pharm. L. Sci.* **2013**, *2,* 562-566.

[33] D. Gao, H. Hu, Y. Wang, W. Yu, J. Zhou, X. Wamg, *Oncol Rep*. **2015**, *34*, 2853-2863.

[34] L. Liu, J. Zhang, M. Li, X. Zhang, J. Zhang, Z. Li, *Mol. Med. Rep*. **2014**, *9*, 2505-2511.

[35] L. Kast, S. W. Sauer, T. Ruppert, T. Beissbarth, M. S. Becker, D. Suss, *FEBS Lett*. **2014**, *588*, 175-183.

[36] N. Cormier, A. Yeo, E. Fiorentino, J. Paxson, *J. Vis. Exp*. **2015**, *106*, 1-9.

Entry for the Table of Contents

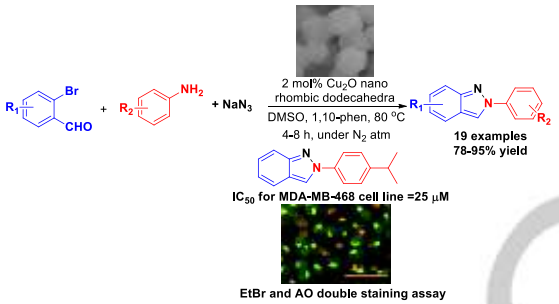

Combination of nanomaterials, heterocyclic synthesis and anti-cancer activity in one-pot. A set of 2*H*-indazole compounds were synthesized by Cu_2O nanoparticles and screened for inhibitory activity against a panel of cancer cell lines such as lung, colon, and breast cancer cell lines. Compound with a isopropyl moiety as the substituent was found to inhibit MDA-MB-468 cells with 25 μM concentration.